

Ice versus liquid water saturation in simulations of the indian summer monsoon

Russell H. Glazer & Vasubandhu Misra

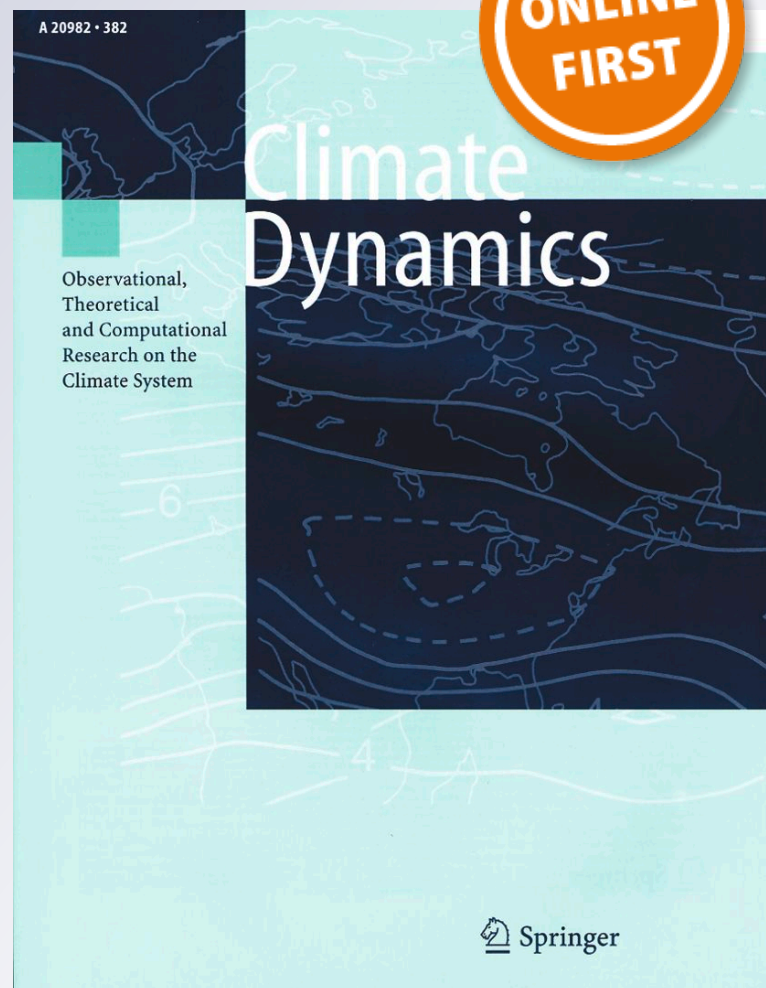
Climate Dynamics

Observational, Theoretical and
Computational Research on the Climate
System

ISSN 0930-7575

Clim Dyn

DOI 10.1007/s00382-018-4116-4



Your article is protected by copyright and all rights are held exclusively by Springer-Verlag GmbH Germany, part of Springer Nature. This e-offprint is for personal use only and shall not be self-archived in electronic repositories. If you wish to self-archive your article, please use the accepted manuscript version for posting on your own website. You may further deposit the accepted manuscript version in any repository, provided it is only made publicly available 12 months after official publication or later and provided acknowledgement is given to the original source of publication and a link is inserted to the published article on Springer's website. The link must be accompanied by the following text: "The final publication is available at link.springer.com".



Ice versus liquid water saturation in simulations of the Indian summer monsoon

Russell H. Glazer^{1,2} · Vasubandhu Misra^{1,2}

Received: 22 May 2017 / Accepted: 29 January 2018
© Springer-Verlag GmbH Germany, part of Springer Nature 2018

Abstract

At the same temperature, below 0 °C, the saturation vapor pressure (SVP) over ice is slightly less than the SVP over liquid water. Numerical models use the Clausius–Clapeyron relation to calculate the SVP and relative humidity, but there is not a consistent method for the treatment of saturation above the freezing level where ice and mixed-phase clouds may be present. In the context of current challenges presented by cloud microphysics in climate models, we argue that a better understanding of the impact that this treatment has on saturation-related processes like cloud formation and precipitation, is needed. This study explores the importance of the SVP calculation through model simulations of the Indian summer monsoon (ISM) using the regional spectral model (RSM) at 15 km grid spacing. A combination of seasonal and multiyear simulations is conducted with two saturation parameterizations. In one, the SVP over liquid water is prescribed through the entire atmospheric column (woIce), and in another the SVP over ice is used above the freezing level (wIce). When SVP over ice is prescribed, a thermodynamic drying of the middle and upper troposphere above the freezing level occurs due to increased condensation. In the wIce runs, the model responds to the slight decrease in the saturation condition by increasing, relative to the SVP over liquid water only run, grid-scale condensation of water. Increased grid-scale mean seasonal precipitation is noted across the ISM region in the simulation with SVP over ice prescribed. Modification of the middle and upper troposphere moisture results in a decrease in mean seasonal mid-level cloud amount and an increase in high cloud amount when SVP over ice is prescribed. Multiyear simulations strongly corroborate the qualitative results found in the seasonal simulations regarding the impact of ice versus liquid water SVP on the ISM's mean precipitation and moisture field. The mean seasonal rainfall difference over All India between wIce and woIce is around 10% of the observed interannual variability of seasonal All India rainfall.

Keywords Indian monsoon · Regional modeling · Saturation vapor pressure · Cloud microphysics scheme

1 Introduction

In numerical models, the calculation of saturation vapor pressure (SVP) in the atmosphere is most typically done through iterations of the Clausius–Clapeyron equation with the input of the local temperature. This is then used to calculate other moisture variables, such as the relative humidity, which are used throughout the model for the specified time step. The SVP calculation is essential because cloud

formation is observed at relative humidities at or very close to saturation (Yau and Rogers 1989). Below the freezing point (0 °C), formation of ice is possible and saturation over ice occurs at a slightly lower vapor pressure than over water. This means that cloud formation will differ depending on whether ice or water is present. However, above the freezing level, clouds are often mixed-phase depending on whether or not ice nuclei are present. Since ice nuclei are less abundant than condensation nuclei (Murray et al. 2012), it is common to find supercooled water drops above the freezing level.

The general convention for radiosonde observations is to report the relative humidity with respect to liquid water throughout the atmospheric column (WMO 1988, 2015a). In a recent World Meteorological Organization (WMO) report (WMO 2015b), it was acknowledged that national practices often differ in the method used to calculate dewpoint and frost point. Observational and theoretical studies of

✉ Russell H. Glazer
rhg11c@my.fsu.edu

¹ Center for Ocean-Atmosphere Prediction Studies (COAPS),
Florida State University, 2000 Levy Avenue, Building A,
Suite 209A, Tallahassee, FL 32306, USA

² Department of Earth, Ocean and Atmospheric Science,
Florida State University, Tallahassee, FL, USA

relative humidity by Korolev and Isaac (2006) and Korolev and Mazin (2003) concluded that in mixed-phase clouds the relative humidity is close to the saturation over water, whereas in ice-phase clouds the relative humidity can be lower than the saturation over ice or supersaturated over ice but is always lower than the saturation over water. A review study by Murphy and Koop (2005) recommended reporting the relative humidity with respect to ice below 0 °C because of the uncertainty in measurements of the vapor pressure of supercooled water. Considering these studies and recommendations, it is apparent that a consistent method for calculating moisture and humidity variables does not yet exist.

Because a substantial portion of the troposphere holds temperatures below the freezing point, the potential impact on a numerical model due to the treatment of saturation in this region should not be ignored. The assumptions made about saturation in the freezing region will affect the water vapor distribution, the cloud amount, the precipitation, and the radiative flux through the atmosphere, regardless of whether the cloud scheme is prognostic or diagnostic. Currently, there is not a consistent treatment of ice and liquid-phase moisture variables in numerical models. Some have specified saturation over water for mixed-phase clouds (e.g., Rotstayn et al. 2000; Tremblay and Glazer 2000), but most use separate temperature conditions to divide the regions where liquid, mixed and ice phase clouds are assumed to form (e.g., Fowler et al. 1996; Moorthi et al. 2001; Slingo 1980; Lohmann and Roeckner 1996). Table 1 compiles a list of the saturation conditions used in five Coupled Model Intercomparison Project Phase 5 (CMIP5) models. Note that the way moisture variables (e.g. relative humidity) are represented in model output, may not reflect how they are treated internally within the model. Table 1 is meant to reflect how the moisture and saturation is treated internally, as it relates to cloud formation for each model. Several models including the National Center for Environmental Prediction (NCEP) Climate Forecast System version 2 (CFSv2), the Geophysical Fluid Dynamics Laboratory (GFDL) AM3, and the National Center for Atmospheric Research (NCAR)

CCSM4 treat the region between 0 and –20 °C as the mixed phase region, and linearly interpolate the SVP from saturation over liquid at 0 °C, to saturation over ice at –20 °C. The NASA GISS ModelE calculates the saturation over water for all layers below –4 °C over the ocean and –10 °C over land, and all layers above –35 °C are saturation over ice. In between a probability exists for either phase but not both (either liquid or ice but not mixed). The reasoning for each temperature condition is tied directly to what cloud phase is assumed to be formed at those temperatures. Note that large differences exist in the assumptions made between the group of models which designate 0 to –20 °C for mixed saturation, and the NASA and Max Planck Institute (MPI) models. While numerous formulations exist to address the basic principle of saturation, relatively little attention has been paid to the potential sensitivity that the treatment of saturation has within a numerical model.

On the other hand, the role that clouds play in climate has received an enormous amount of attention since the satellite era began. Relative to a cloud-free atmosphere, clouds cool the mean global climate by increasing Earth's albedo and reflecting incoming solar radiation back to space, and warm the mean global climate by absorbing and trapping longwave radiation emitted from Earth (Ramanathan 1987). Ramanathan et al. (1989) demonstrated that in our current climate, albedo and solar effects are larger than the heat trapping longwave effects, thus clouds have a net cooling effect on the global climate. How these effects change with a warmer climate is referred to as the "cloud radiation feedback". Many authors have identified the cloud radiation feedback as one of the most important remaining questions in understanding and modeling future climate change (Dessler 2010; Stephens 2005; Bony et al. 2015; Randall et al. 2007). Additionally, the relative composition of hydrometeors and liquid versus ice content within clouds has a strong impact on radiative fluxes through the atmosphere (Matus and L'Ecuyer 2017). The representation of cloud ice and its thermodynamic and radiative properties in climate models could be a cause for remaining uncertainties in modeling future climate change

Table 1 Climate model SVP parameterizations

| Model | Liquid | Mixed | Ice |
|---|--|--|---------------------|
| CFSv2 Saha et al. (2014) | $T > 0\text{ °C}$ | Linearly interpolate between liquid and ice for $0\text{ °C} > T > -20\text{ °C}$ | $T < -20\text{ °C}$ |
| GFDL-AM3 Donner et al. (2011) | $T > 0\text{ °C}$ | Linearly interpolate between liquid and ice for $0\text{ °C} > T > -20\text{ °C}$ | $T < -20\text{ °C}$ |
| NASA-GISS ModelE Schmidt et al. (2014) | If over ocean, $T > -4\text{ °C}$, if over land, $T > -10\text{ °C}$ | Probability exists for either phase if over ocean and, $-4\text{ °C} > T > -35\text{ °C}$ or over land if $-10\text{ °C} > T > -35\text{ °C}$ | $T < -35\text{ °C}$ |
| CCSM4 Meehl et al. (2012) | $T > 0\text{ °C}$ | Linearly interpolate between liquid and ice for $0\text{ °C} > T > -20\text{ °C}$ | $T < -20\text{ °C}$ |
| MPI-ESM Giorgetta et al. (2013) | $T > -35\text{ °C}$ | Saturation over liquid water assumed | $T < -35\text{ °C}$ |

(Waliser et al. 2009, 2011; Su et al. 2011). A recent study by Tan et al. (2016) reported a major source of uncertainty in CMIP5 climate projections that is attributed to inaccuracies in the production of ice in mixed-phase clouds from the CMIP5 model schemes. A major source of ice crystal growth within mixed-phase clouds is the Wegener–Bergeron–Findeisen (WBF) process (Pruppacher and Klett 1978) whereby ice grows at the expense of liquid water in a mixed phase cloud. SVP between that over ice and that over liquid water is a necessary but not sufficient condition for ice crystal growth by WBF in mixed-phase clouds.

The ISM is one of the dominant yearly tropical circulations and has far-ranging teleconnections to regions from the equatorial east Pacific to east Africa and the Arabian Deserts (Webster et al. 1998). The ISM provides upwards of 80% of the annual rainfall for the Indian subcontinent and thus India's agricultural and economic well-being are closely tied to the ISM (Parthasarathy et al. 1994). With nearly a quarter of the world's population living within this monsoon region, the importance of studying the ISM cannot be overstated, especially in light of longstanding difficulties with modeling the ISM (Waliser et al. 2003; Sperber et al. 2012; Sabeerali et al. 2014). However, significant progress has been made recently to improve the resolution and parameterization of clouds and their microphysics in the CFSv2 (Abhik et al. 2017; Ramu et al. 2016; Goswami et al. 2015), which is currently used operationally at the India Meteorological Department (IMD) for seasonal ISM forecasting. As a result of improvements to the cloud representation in the CFS, Abhik et al. (2017) and Goswami et al. (2015) found improved propagation of the ISM intraseasonal oscillation and its associated rainfall signature. In addition, several recent studies have documented the importance of the ISM's cloud characteristics for understanding the observed rainfall patterns (Kumar et al. 2014) and the propagation (Jiang et al. 2011; Abhik et al. 2013; Wang et al. 2015) and identification of intraseasonal oscillations (Rajeevan et al. 2013).

For this study, we conducted seasonal and multiyear simulations of the ISM using the regional spectral model (RSM; Juang and Kanamitsu 1994; Kanamitsu et al. 2010) in order to understand how the representation of ice and liquid water saturation within a climate model reflects upon the mean seasonal ISM. The authors believe the ISM region to be ideal for a study such as this because of the enormous amount of rainfall, convection and water vapor that is present during the monsoon, especially in the upper atmosphere (Gettelman et al. 2006). The focus of this model experiment is based on a comparison of simulations where SVP over ice above the freezing level is calculated (wIce), with an identical set of simulations where SVP over liquid water is calculated throughout the atmospheric column (woIce). The calculation of SVP filters down to all other moisture variables such that we anticipate the first order effect from the difference in

SVP in the two sets of simulations to be seen in the moisture field. We expect that an important second order effect will be observed in cloud distributions of model layers that lie above the freezing level. Here, we emphasize that the scope of this study is limited to an evaluation of the impact that the SVP calculation has on the seasonal mean ISM representation in the model. In some cases, vastly different assumptions are made regarding SVP in numerical models currently used, including the climate models shown in Table 1. To date, there has not been an attempt to understand the implications of different saturation assumptions above the freezing level and the effect this may have on a model's humidity distribution, precipitation, cloud amount, and radiative flux.

The layout of this paper is as follows: in Sect. 2 we provide the RSM's setup, the experimental design, and a description of the cloud scheme used in the model including a discussion of how this is important for the study. A verification of the methodology used to calculate the SVP over water and ice in the two separate sets of simulations is also provided in Sect. 2. Section 3 begins with a comparison of the mean seasonal cloud layer amount and precipitation from the seasonal simulations with observational data. We then assess the differences in the mean seasonal moisture and temperature between the wIce and woIce simulations. That is followed by a discussion of the effects on cloud distributions and radiative fluxes, and finally, the results from the multiyear wIce and woIce experiments are shown in the context of the impact of the imposed SVP changes. The degree to which the multiyear simulations and seasonal simulations are consistent in terms of the impact from SVP changes is discussed. A summary and conclusions are provided in Sect. 4.

2 Data, model setup, and experimental design

2.1 Model and experimental setup

The regional spectral model (RSM; Juang and Kanamitsu 1994; Kanamitsu et al. 2010), originally developed at the National Center for Environmental Prediction (NCEP), is used in all model simulations for this study. The RSM uses a spectral method to evaluate the primitive equations. Previously it has been used in a host of regional climate studies (Stefanova et al. 2012; Li et al. 2013a, b; Li and Misra 2014). This study focuses strictly on the impact in the RSM simulation with prescribed SST and includes no coupling to an ocean model.

For this study, seasonal simulations were conducted for the period May 1–October 15 for 5 separate years (2001, 2003, 2005, 2012 and 2013). These years were selected because neutral El Niño Southern Oscillation (ENSO)

conditions were present in the Niño 3.4 region (5°S–5°N and 170°–120°W) and it was desirable to avoid possible influence on the ISM from an ENSO event (Rasmusson and Carpenter 1983; Webster et al. 1998). It is, however, recognized that the ISM exhibits interannual variability from other sources such as Indian ocean dipole (IOD) (Ashok et al. 2001; Saji et al. 1999), Himalayan mountain snow pack (Hahn and Shukla 1976) and internal variations of the ISM itself (Krishnamurthy and Shukla 2000, 2007; Goswami 1998). Influence from these conditions on our model results cannot be ruled out, however we have mitigated the influence of ENSO on the ISM through the selection of these 5 neutral years.

For each season we conducted two simulations, each with a different SVP parameterization. In one, the SVP was calculated with respect to liquid water in all model layers where the temperature is greater than 0 °C, and then for all layers above the freezing level (below 0 °C), calculated with respect to ice. These simulations are referred to as wIce (“with ice”). In a second set, the SVP was calculated with respect to liquid water throughout the atmospheric column. These simulations are referred to as woIce (“without ice”). A total of ten seasonal simulations were carried out. The method used to calculate the SVP follows Marx (2002). This method offers high accuracy outside the observed atmospheric temperature domain while maintaining a high level of computational efficiency. It was noted in Shimpo et al. (2008) that there are discrepancies between parameterizations in the RSM and the method used for calculating relative humidity and SVP. For this study, the method used for calculating SVP (and relative humidity) was implemented throughout the model and all of its parameterizations so that it is consistent. In addition to seasonal runs, two 13-year simulations were conducted from 2001 to 2013 using the same domain configuration and boundary conditions as the seasonal runs. One of these multiyear runs used the wIce parameterization and the other used the woIce parameterization.

The model domain chosen for this study (Fig. 1) encompasses the major features of the ISM region and provides a sufficient area over which to simulate the ISM. The horizontal grid spacing is 15 km with 28 terrain following sigma-coordinate vertical levels that are identical to those used by the NCEP-DOE reanalysis (R2; Kanamitsu et al. 2002). The shortwave and longwave radiation schemes used are Chou (1992) and Chou and Suarez (1994) respectively. For the convection scheme, the RSM uses a Relaxed Arakawa–Schubert scheme (Moorthi and Suarez 1992). Atmospheric boundary conditions were provided by NCEP R2 reanalysis (Kanamitsu et al. 2002) along with daily updated optimum interpolation sea surface temperature (SST; Reynolds et al. 2007) data for the ocean boundary conditions. The RSM utilizes a scale selective bias correction (SSBC; Kanamaru and Kanamitsu 2007), which prevents the model on the largest

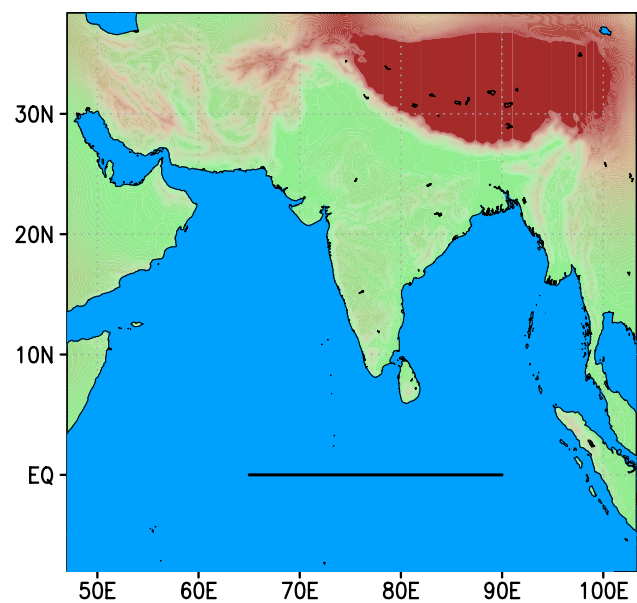


Fig. 1 Model domain used for all simulations in this study. Darker shades of brown indicate increasing height of topography. The solid black line along 65°E–90°E indicates the grid points used to construct Fig. 2

spatial scales resolved within the regional model, from deviating from the large-scale lateral boundary conditions (in this case R2 reanalysis).

2.2 Observational datasets

In addition to the ocean and atmospheric datasets used for boundary conditions in these model simulations, we also utilized several observational datasets for comparison and validation of the model results. The Global Precipitation Climate Project (GPCP) version 1.2 (Huffman et al. 2012) monthly mean (2.5° by 2.5°) rainfall data, for the period 1997–2006, were used for validation with the model’s seasonal mean rainfall. For the same period, daily outgoing longwave radiation (OLR) (Liebmann and Smith 1996) retrievals from the advanced very high resolution radiometer (AVHRR) were used for comparison with modeled seasonal OLR. NCEP R2 reanalysis winds and specific humidity were also used in validating and analysis of model results.

Because of the direct relevance of cloud distribution and statistics to this study, it was important to evaluate the modeled cloud statistics against an observational dataset and to understand what the observed mean cloud distribution should look like during the ISM. For this purpose, two widely used satellite datasets of cloud statistics: the International Satellite Cloud Climatology Project (ISCCP; Rossow and Schiffer 1991, 1999) and the moderate resolution imaging spectroradiometer (MODIS) are available. While both datasets are reliable choices for resolving the

column-integrated cloud field (total cloud), it was pointed out by Chang and Li (2005) that ISCCP has difficulty detecting the cloud tops of layered or overlapped clouds when, for instance, thin high cirrus clouds overlay thicker low clouds. MODIS attempts to improve upon the detection of these thin cirrus clouds by using CO₂ slicing (Platnick et al. 2003). For these reasons, we chose to use the layered-cloud and column integrated cloud amounts provided by MODIS level 3 daily data (Platnick et al. 2015) for comparison with modeled clouds.

2.3 Cloud scheme

For this study, the RSM uses a cloud scheme based on Slingo (1987), Slingo and Slingo (1991) in which cloud fraction is diagnosed at each grid cell based on atmospheric conditions that are physically relevant to cloud formation such as, relative humidity, vertical velocity, and inversion strength in the case of low level clouds. Slingo (1987) groups clouds into four categories, three of which are based on height (i.e., low, medium, high) and a fourth for convective clouds. For low, middle, and high clouds diagnostic equations for the cloud amount as a function of the mean background relative humidity of a grid cell are in the form:

$$C = \left(\frac{RH - RH_c}{1 - RH_c} \right)^2, \text{ for } RH > RH_c \tag{1}$$

$$C = 0, \text{ for } RH \leq RH_c$$

where C is the cloud amount, RH is the mean relative humidity in the grid cell, and RH_c is the critical relative humidity. RH_c is set to 0.85 for high clouds over land and ocean, 0.65 for middle clouds over land, 0.85 for middle clouds over ocean, 0.9 for low clouds over land, and 0.7 for low clouds over ocean. For low clouds, there are two additional parameterizations to account for the possible presence of boundary layer inversion type clouds or low level clouds associated with synoptic scale disturbances, but these will not be discussed in detail here. Convective clouds can occupy any of the three other levels and the amount comes directly from the convection scheme.

It is recognized that the use of a diagnostic cloud scheme in this case may have disadvantages. For one, the absence of prediction of cloud water or ice is limiting in the detail by which the cloud amount is calculated as well as the representation of precipitation that is not convective in nature. Further, the large-scale precipitation in RSM is produced from the instant removal of supersaturation. We argue, however, that the advantages to using a more detailed prognostic cloud water scheme are small here. In a study of four cloud schemes (one of which was Slingo) in the G-RSM (Global-RSM), Shimpo et al. (2008) found little benefit to

using a prognostic cloud scheme. They concluded that no single cloud scheme could be distinguished from the others as clearly better performing. Shimpo et al. (2008) recommended improvements to several common cloud water prediction schemes on account of their poor representation of cloud water relative to observations. Furthermore, in a study of three cloud prediction schemes, one being the Slingo scheme, and another being the Xu and Randall (1996) prognostic cloud water scheme, Wood and Field (2000) found that the Slingo scheme performs relatively well in terms of cloud amount when compared to observations and the Xu and Randall scheme. While a prognostic cloud scheme with additional parameterizations for cloud microphysical processes that are not included in a diagnostic scheme like Slingo is preferable, we argue that these additional processes may not have direct relevance to the SVP calculation. Relative humidity on the other hand, is clearly and quite directly affected by the SVP. We would then argue that a cloud scheme that determines cloud amount mainly as a function of relative humidity is the most direct way of testing the impact of SVP on cloud distribution qualitatively. Essentially, we offer this experiment using the Slingo scheme as an initial step toward understanding the affect that SVP has on a numerical simulation. Still, we recognize that the benefits of a more detailed representation of cloud microphysical processes would offer a more complete test, and we are exploring additional experiments with more complex cloud schemes that will be reported in a future study.

2.4 Verification of ice vs. liquid water relation

Before entering into an analysis of the model results, it is important to first understand the theory behind the changes that have been made to the model and to verify that the model is indeed producing what we expected from the changes made to the calculation of SVP. The theoretical difference between the wIce and woIce simulations were how SVP was calculated above the freezing level. This is understood through the Clausius–Clapeyron relation which is used to calculate SVP in the model.

$$e_s = \epsilon e^{r_v \left(\frac{1}{T_0} - \frac{1}{T} \right)} \tag{2}$$

$$e_{si} = \epsilon e^{r_v \left(\frac{1}{T_0} - \frac{1}{T} \right)} \tag{3}$$

Equations (2) and (3) are Clausius–Clapeyron relations for calculating SVP over water and ice, respectively, where e_s is the SVP over water, e_{si} is the SVP over ice, T₀ is the freezing point (273.15 K), T is the environmental temperature, r_v is the gas constant for moist air, and ε is the vapor pressure at temperature T₀. l_v and l_s are the latent heat of vaporization and sublimation respectively. Equation (2) is

then representative of SVP calculation in the woIce runs and Eq. (3) is representative of SVP calculation in the wIce runs, above the freezing level. We can verify this by plotting the model derived SVP and corresponding temperature in the wIce and woIce runs along with the theoretical Clausius–Clapeyron relation for ice and liquid water (Fig. 2a). We expect that the SVP derived in the wIce runs should follow the theoretical curve for SVP over ice and that the SVP derived in the woIce runs should follow the theoretical curve for SVP over liquid water. In general, this was the case as shown in Fig. 2a. Taking the hourly model derived SVP and temperature from grid points along an equatorial cross section, we found that the points from wIce and woIce were very closely clustered around their respective Clausius–Clapeyron relation. The SVP from the model shown here will not exactly follow the Clausius–Clapeyron relation for a few reasons: (1) the SVP is inferred from the specific humidity (q) and relative humidity, so it is not the exact SVP from the model at that timestep and (2) the output from the model is interpolated to pressure levels from the native sigma levels.

We are also interested in the difference in SVP between wIce and woIce on hourly timescales because this will have direct implications for differences in cloud formation between wIce and woIce. The difference in SVP will also be important for beginning to understand how sensitive the model is to the SVP calculation. Figure 2b shows the difference in SVP (for a given temperature) between wIce and woIce from model levels at the same locations as in Fig. 2a. The theoretical difference in SVP from Clausius–Clapeyron is also shown for comparison. Notice that the greatest theoretical difference in SVP for ice and liquid water is at -12.5°C . Notice also that the data in Fig. 2b (and Fig. 2a) are clustered according to the model level that they are taken from and that, in this case, there are three clusters for this temperature range that correspond to 500, 400 and 300 mb. The greatest difference in SVP is then theoretically between 400 and 500 mb in the atmosphere for this equatorial region. The data from the 300 mb level generally follows the theoretical relation closely while grid points near the max SVP difference at -12.5°C shows greater variability. In general, it seems that the departure of the model from the theoretical SVP difference increases near the maximum difference at -12.5°C .

3 Results and discussion

3.1 Comparison with observations

We expect that, because of changes made to the calculation of SVP in the model experiments and by association the moisture and relative humidity, the model cloud-layer fields will differ between wIce and woIce, especially in the middle

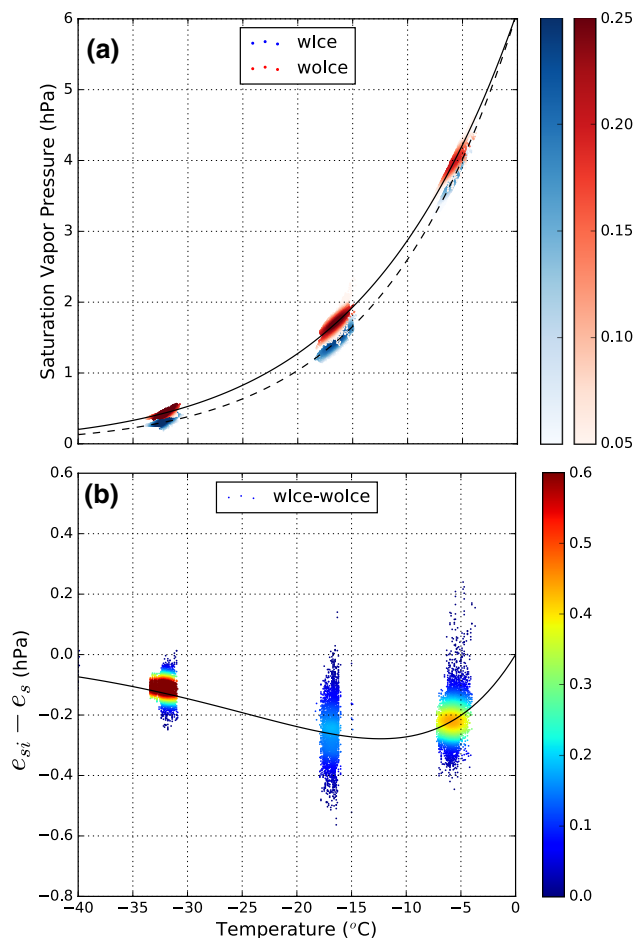


Fig. 2 **a** The SVP (hPa) plotted with the temperature of grid points taken from the region indicated in Fig. 1. Red dots indicate data from grid points in the woIce simulation while blue dots indicate data from the wIce simulation. The dotted black line indicates the SVP calculated with respect to ice using the Clausius–Clapeyron relation and the solid black line indicates the SVP calculated with respect to water using the Clausius–Clapeyron relation. **b** The difference in SVP ($e_{\text{ice}} - e_{\text{water}}$) plotted with the corresponding temperature at grid points taken from model simulations at the same locations as in (a). The solid black line in **b** indicates the difference of SVP calculated with respect to ice minus the SVP calculated with respect to water using the Clausius–Clapeyron relation. The shading of the points in **a** and **b** indicate the probability density function of the data using a Gaussian kernel density estimation. Higher probability density values indicate greater clustering of the data. All data are gathered in both simulations from 00z May 29 to 00z May 31 2001 at hourly intervals. Note that model output is in pressure levels and data are clustered into three groups which correspond to 500, 400, and 300 mb

and high cloud regime where most the atmosphere is below 0°C . To start, we evaluated the modeled high, middle, low and total cloud fields against the satellite derived fields from MODIS. It is important to note, however, that the cloud layer and total cloud amounts from RSM are calculated using a maximum-random overlap assumption while MODIS cloud fields were derived from the satellite's top-down view from space with no assumptions about cloud overlap. Therefore,

to facilitate comparison with MODIS, the model cloud layer fields were transformed to mimic a top-down view of the cloud layers following the method of Weare (2004) and Shimpo et al. (2008). For modeled high clouds, the amount is theoretically the same as that seen from space by MODIS. For middle clouds, the amount “as seen from space” is equal to the model derived middle cloud amount minus the high cloud amount that obscures the middle clouds using a “random overlap assumption.” This can be expressed in the following relation:

$$\text{mid_asfs_cf} = \text{mid_cf} * (1 - \text{high_cf}) \quad (4)$$

where high_cf is the model-derived high cloud amount, mid_cf is the model-derived middle cloud amount and mid_asfs_cf is the middle cloud amount as seen from space in the model. The low cloud amount that is as seen from space is then the model derived low cloud amount that is not obscured by middle or high clouds, or

$$\text{low_asfs_cf} = \text{low_cf} * (1 - \text{mid_cf}) * (1 - \text{high_cf}) \quad (5)$$

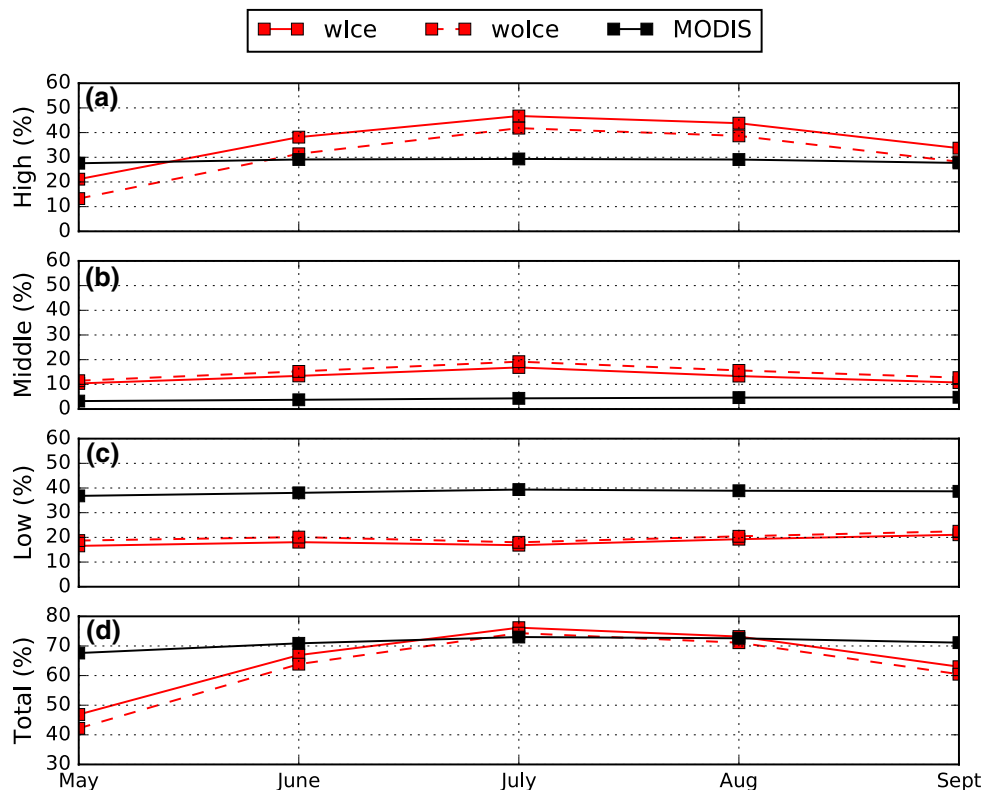
where low_cf is the model-derived low cloud amount and low_asfs_cf is the low cloud amount as seen from space in the model.

Utilizing the relations above, we compared the mean monthly May–September cloud layer and total cloud amounts from the seasonal simulations with MODIS in

Fig. 3. Both the modeled clouds and MODIS follow the monsoon seasonal cycle with a steady increase in cloud amount from May–June in the lead up to onset, and a peak in cloud amount occurring in July that coincides with the peak of the monsoon season before a decrease in clouds and convection from August–September. The model simulations generally showed more monthly variability than MODIS, especially with respect to high cloud amount. The model overestimated the high cloud amount during the peak of the monsoon season with respect to MODIS. This may be a symptom of the high cloud amount being sensitive to the activity of the convective parameterization. The middle cloud amount was also overestimated in the model, and showed greater seasonality than MODIS, while the low cloud amount was the only layer underestimated. Li and Misra (2014) also noted a bias for underestimation of low clouds in the RSM. With respect to total cloud amount, again we found strong seasonality in the model clouds which leads to underestimation outside of the peak monsoon months.

In comparing the wIce and woIce mean cloud amounts, we found the largest difference in the middle and high clouds where the high cloud amount in wIce was consistently larger by 5–7%. Middle clouds, however, were fewer in the wIce simulations by 1–3%. The total column cloud layer amount increased in wIce due mainly to the significant increase in high clouds. It is worth noting that the mean

Fig. 3 Monthly area averaged **a** high, **b** middle, **c** low, and **d** total cloud fraction (%) during ISM months over the ISM region, 5°S–25°N and 60°E–95°E. The mean of the five seasonal wIce and woIce simulations are represented in the red solid and red dashed lines respectively. MODIS monthly cloud fraction data averaged over a 13-year period (2002–2015) are represented with a solid black line. The middle and low cloud amounts from the model are transformed to be “as seen from space” to facilitate comparison with MODIS



cloud differences between wIce and woIce were nearly uniform across the monsoon season and did not change sign.

To evaluate the mean monsoon in the model simulations, we compared the model's June, July, August, September (JJAS) mean rainfall, OLR, and 850 hPa circulation with observations during the 10-year period 1997–2006 in Fig. 4. The model simulations tended to precipitate more in the inter-tropical convergence zone (ITCZ) region over the Equatorial Indian Ocean than in the GPCP observations. Over land, the model simulations and GPCP rainfall were in better agreement and the two main precipitating regions over the Western Ghats and Myanmar coast were easily identifiable in the model. It is clear from Fig. 4 that the mean seasonal rainfall in wIce and woIce appears very similar and that a closer analysis is needed (addressed in Sect. 3.4).

3.2 Moisture and thermodynamics

The distinction between wIce and woIce is in the calculation of SVP above the freezing level. Therefore, it is important to first locate the freezing level and determine its spatial variability in the ISM region. Figure 5a shows the JJAS mean freezing level across the model domain for the wIce simulations. We found that there was little difference in the height of the freezing level between wIce and woIce (not shown), and thus Fig. 5a can be taken as representative of both simulations. In general, the freezing pressure level decreases (increases in height) from south to north across the domain but remains between 600 and 500 hPa. Coincident with this rise in the freezing level was an increase in seasonal mean specific humidity (q) between the 600 to 500 hPa layer in the R2 reanalysis forcing (Fig. 5b). It follows then that the potential change in saturation is greater over India and the Bay of Bengal (BoB), where there is a maximum in q , when saturation over ice is calculated instead of over liquid water. To consider whether this was indeed the case, Fig. 6 shows a zonally-averaged cross-section of the difference (wIce-woIce) in mean relative humidity, q and temperature with height for the JJAS period during the model simulations. A clear relative drying at the freezing level was apparent in the wIce simulations from the RH and q profiles (Fig. 6a, b). The maximum in relative drying from 10°N to 20°N between 500 and 600 hPa is a consequence of a coincident maximum in available moisture over India and the BoB. The amount of drying with respect to q decreased with height (Fig. 6b) because there is generally less water vapor with increasing height. A portion of the drying is also observed in q and RH below the mean freezing level. The reasons for this relative drying are related to two processes which involve convection. First, when vigorous convection occurs, condensation and rainfall will be increased above the freezing level in wIce relative to woIce. Precipitation will fall into the layers below the freezing level which will then trigger those

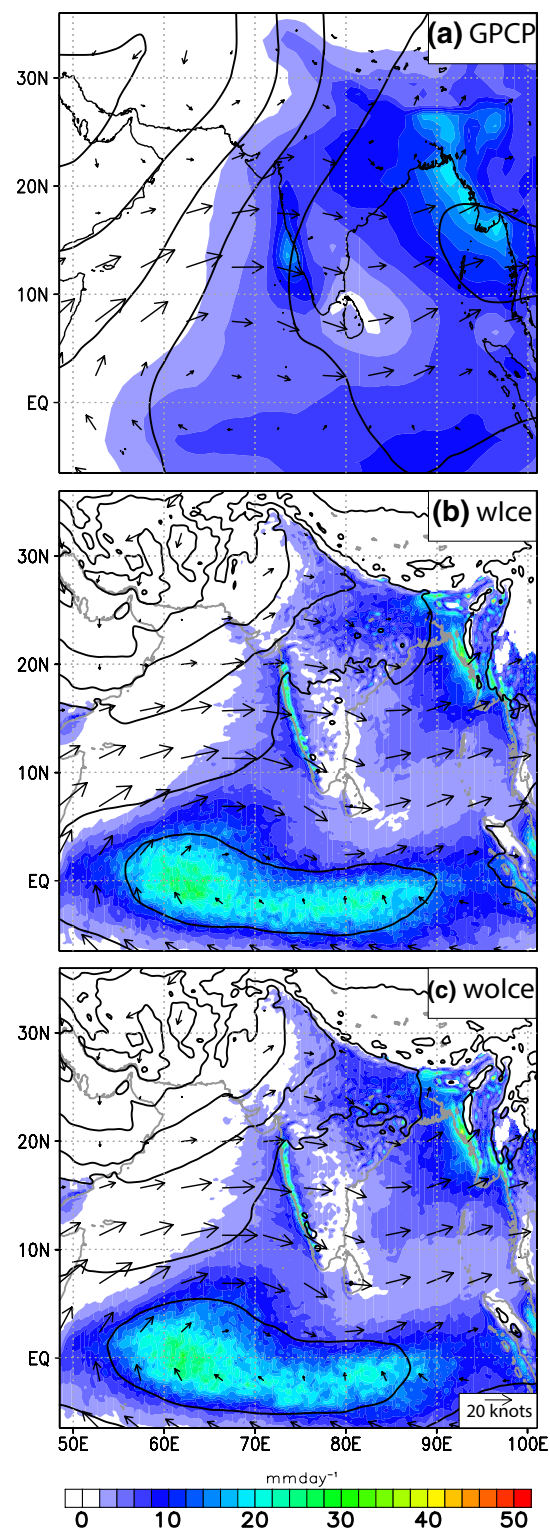


Fig. 4 a GPCP daily rain rate (mm/day) shaded, R2 850 hPa wind vectors (knots), and AVHRR satellite derived OLR (W/m^2) averaged over JJAS for the 10-year period 1997–2006. And JJAS mean rain rate, OLR, and 850 hPa wind vectors for the five seasonal model simulations **b** wIce and **c** woIce; the contour interval for the OLR is 20 W/m^2 . Precipitation over high terrain (the Himalayan mountains) is removed

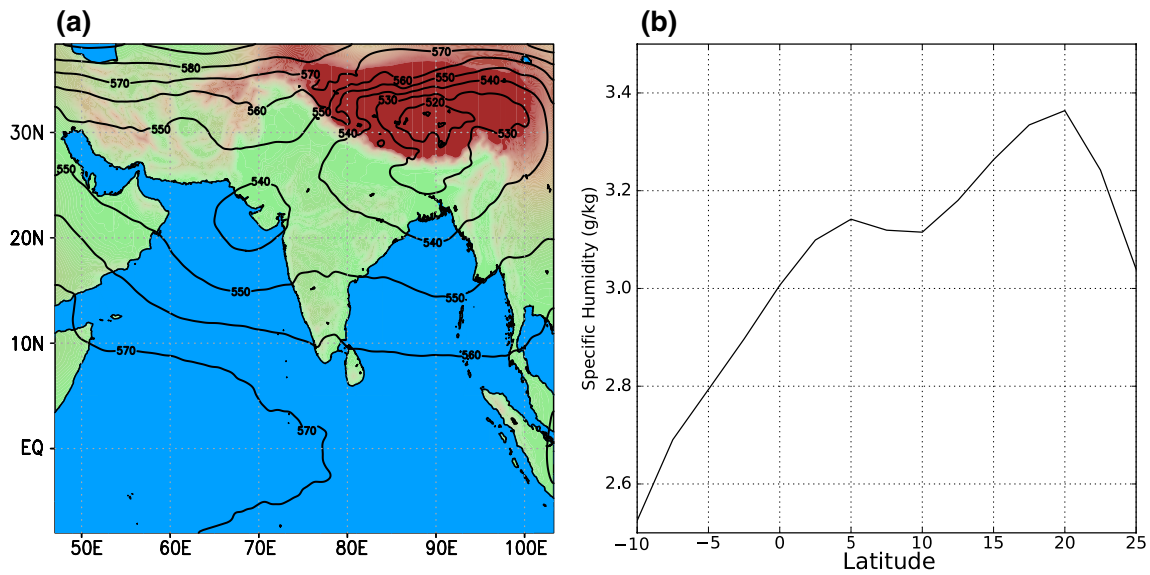


Fig. 5 **a** JJAS mean height of the freezing level (0 °C) in pressure (hPa) from the 5 wIce simulations. **b** Zonally averaged (50°E–100°E) 500–600 hPa mean specific humidity (g/kg) during JJAS for the years 2000–2007 in R2 reanalysis

layers, which are already close to saturation, to consequently condense and precipitate as well, thereby removing moisture from the column below the freezing level. A second process which can lead to drying below the freezing level is large-scale subsidence in association with convection. In the wake of convection, large-scale subsidence may bring relatively dryer air above the freezing level down to the layers adjacent to the convection below the freezing level. This is the result of condensation and rainfall occurring in the model levels above, precipitating into the layers below the freezing level, which then triggers those layers to saturate from evaporation of falling precipitation and consequently condense, serving as a moisture sink. For these layers below the freezing level, the seasonal mean water vapor removed as a result of condensation, and precipitation, and large-scale subsidence is greater than the addition of water vapor from evaporation into unsaturated layers.

As soon as the freezing level is crossed in wIce simulations, the saturation-specific humidity is dropped to be over ice. This means that the air will immediately be closer to saturation and, in some cases, may be supersaturated in the layers near the freezing level. With little change in the moisture advection and overall mean circulation between the wIce and woIce runs, the changes in the tendency of q between the two model simulations is then a function of precipitation and condensational processes. Any water vapor that condenses in the model is assumed to fall out as precipitation, leading to a decrease in q . In addition, any supersaturation is immediately removed in the model and converted to precipitation. It seems apparent then that the response of the wIce simulations to the slight decrease in SVP is to

increase the grid-scale condensation and in doing so adds to a preexisting moisture sink in the model.

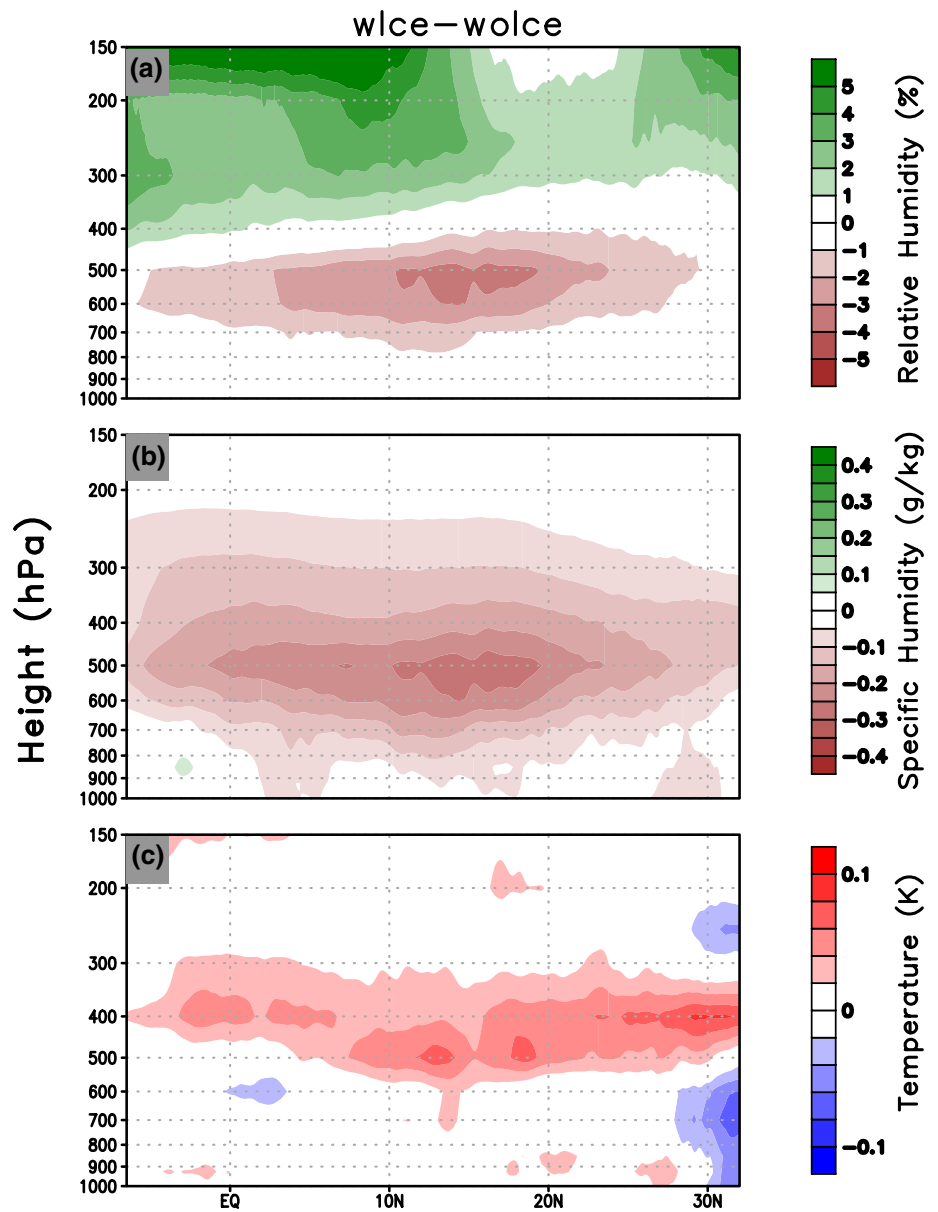
The difference in temperature (Fig. 6c) shows slight warming in the mid to upper troposphere which is located slightly above the freezing level and the region where maximum drying is occurring in wIce. The warming appears significant because it is consistent from south to north between 400 and 500 hPa. Diabatic latent heat released due to increased condensation may be the cause of warming in the mid and upper troposphere but this cannot be confirmed without a profile of diabatic heating and cooling, which was not accessible from the model simulations in this study. Also note that for this study modifications are only made to the SVP calculation. The latent heat of condensation for warm and cold rain processes continue to be included in both (wIce and woIce) runs.

Recognizing that the SSBC in the model may affect the results described here, the model simulations wIce were repeated without the SSBC and similar qualitative results were found (not shown).

3.3 Clouds and radiation

Figure 7 shows the spatial variability of the difference in the mean seasonal low, middle, high and total cloud amount between wIce and woIce. A decrease in middle cloud fraction can be seen (Fig. 7b) over most of the domain in wIce, which coincides well with the decrease in RH near the freezing level seen in Fig. 6a. Conversely, Fig. 7c shows an increase in high cloud amount over most of the ISM region with a maximum in the eastern equatorial Indian

Fig. 6 Zonally averaged (50°E–100°E) cross-section of **a** relative humidity (%), **b** specific humidity (g/kg) and **c** temperature (K) difference relative to wIce (wIce-wolce) averaged over all model years during JJAS. Temperature contour interval is 0.02 °C



Ocean (EEIO) and BoB. The total cloud amount (Fig. 7d) is calculated as the maximum cloud coverage found out of the three cloud level categories, or total = max(low, middle, high). Since the high cloud amount is often the largest out of the three layers, any increase in the high cloud amount will generally lead to an increase in the total cloud amount. In Fig. 7d we observed an increase in total clouds over most of the region where the high clouds increased but over India where middle clouds are significantly decreased, the change to total clouds is negligible.

In the mean seasonal cloud field two distinct regimes emerge: one over the EEIO and southern BoB where an increase in high clouds occurs in the wIce runs, and another over India and the Arabian Sea where high clouds also increase but middle clouds decrease by a similar or

greater amount in the wIce runs. Because of the strong coupling between clouds and radiation we see these regimes manifesting in the mean radiation fluxes shown in Fig. 8. For example, we observe that in the wIce run, at the surface, shortwave (SW) radiation is decreased over the EEIO as a result of increased high clouds, which adds to Earth's albedo relative to the wolce run. To understand the increase in SW radiation over the Arabian Sea and India in Fig. 8a it is important to know that stratiform clouds are parameterized to be more optically thick than cirrus clouds. In this case the middle clouds are mostly stratiform to the model and high clouds are cirrus type. This means that the SW radiation flux will be more sensitive to changes to the middle cloud amount. Because

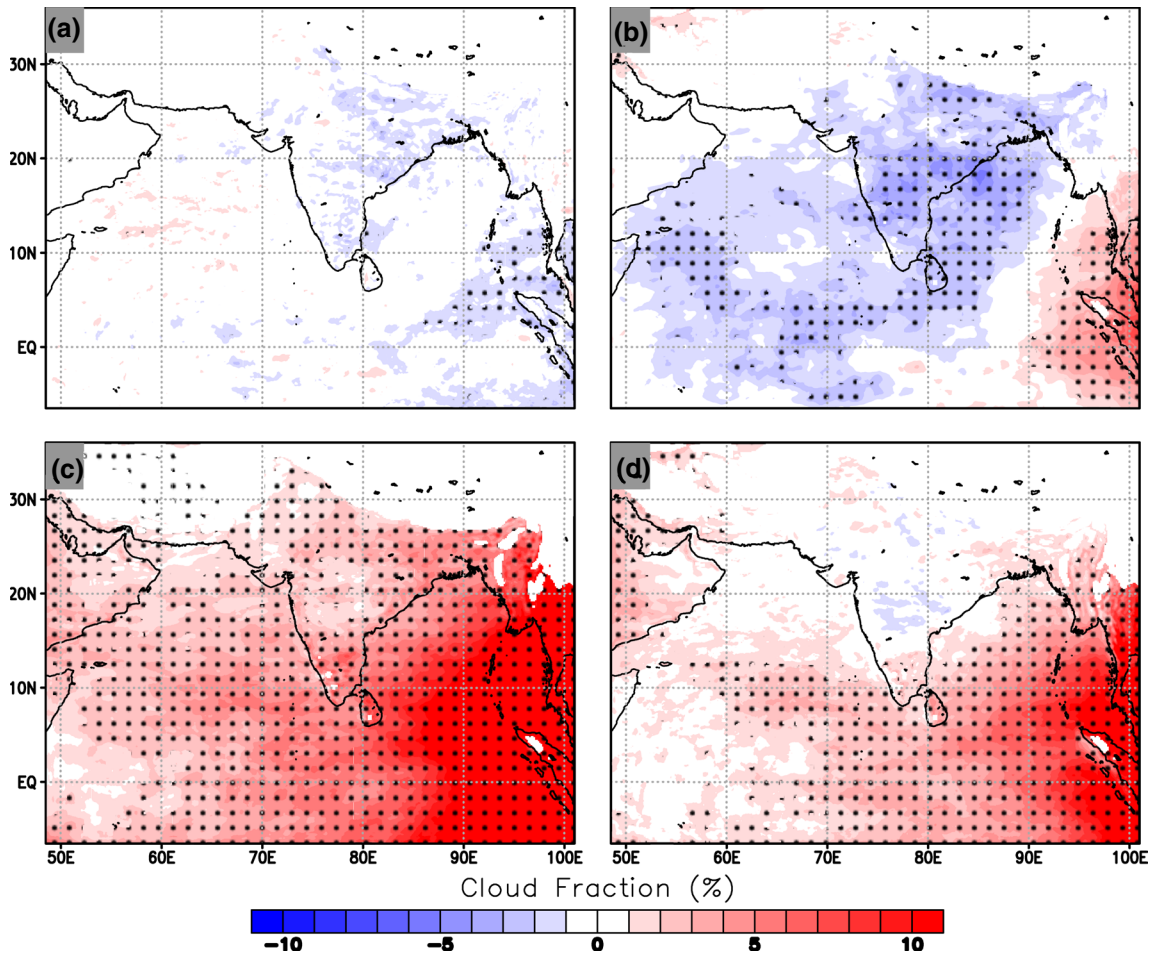


Fig. 7 Shaded **a** low, **b** middle, **c** high and **d** total cloud fraction (%) difference relative to wIce (wIce-wIce) averaged over all model years during JJAS. Red indicates an increase in cloud fraction over

JJAS, whereas blue indicates a decrease. Statistically significant values at the 90% confidence interval are dotted. Data over high terrain is not shown

the middle cloud amount decreases over the Arabian Sea and India in the wIce run, less SW radiation is absorbed in the atmosphere despite a similar magnitude increase in high clouds and thus an increase in surface SW flux is observed there. In terrestrial longwave (LW) radiation, clouds both absorb LW radiation from Earth's surface and emit LW to space and downward toward Earth. Because of the increase in SW radiation over the Arabian Sea and India in the wIce runs, the mean land surface temperature over India is slightly increased (not shown) and thus a net increase in outgoing LW radiation leaving the surface is observed (Fig. 8). Due to emission by clouds, the increase in clouds over EEIO in the wIce runs resulted in a gain in LW radiation at the surface. At top of the atmosphere (TOA; Fig. 8c, d) a loss can again be seen in SW over the EEIO as more SW is reflected back to space, while a gain in SW radiation is felt over the Arabian Sea and India,

consistent with the relative changes in cloudiness in the wIce runs.

3.4 Seasonal rainfall characteristics

In Sect. 3.2 it was found that the switch to saturation over ice above the freezing level in the wIce simulations caused a removal of moisture in the mid and upper troposphere. This removal of moisture suggests increased grid-scale condensation and conversion to rain within the model when saturation over ice is applied. It then follows that we should, in a seasonal mean sense, observe an increase in the amount of rainfall coming from the model's cloud scheme and not by the sub-grid-scale convective parameterization. This was investigated in Fig. 9 where the percentage contribution to the total mean seasonal rainfall from the grid-scale precipitation in wIce and wIce is shown. Since the total precipitation is made up of two components: grid-scale

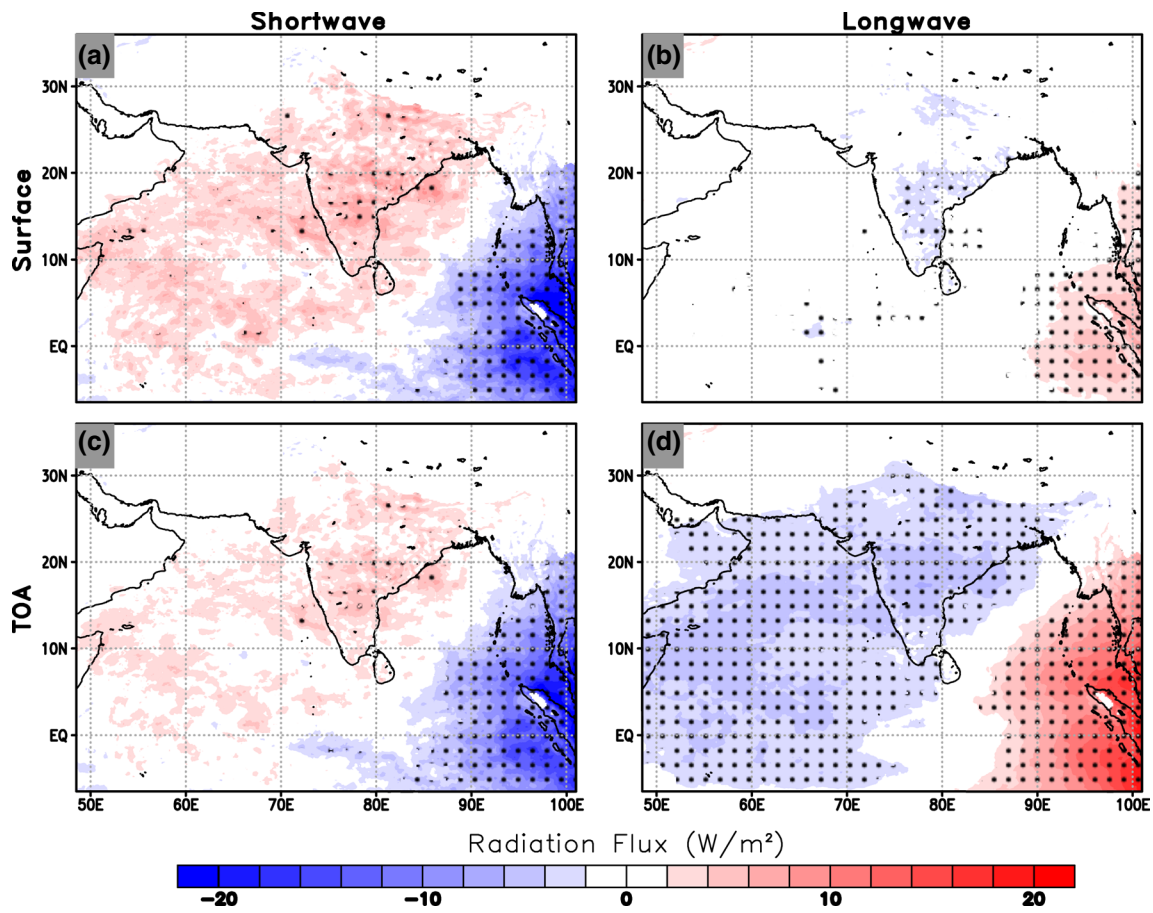


Fig. 8 Model mean JJAS difference (wIce-woIce) for **a** shortwave radiation flux at the surface and **c** top of the atmosphere (W/m^{-2}) and **b** the longwave radiation flux at the surface and **d** top of the atmosphere (W/m^{-2}). Here positive values indicate that the change in flux is downwards (gain) and negative values indicate that the change in

flux is upward (loss). The calculation of the flux before differencing is also done with the same convention: upwards is negative (loss), downwards is positive (gain). Statistically significant values at the 90% confidence interval are dotted

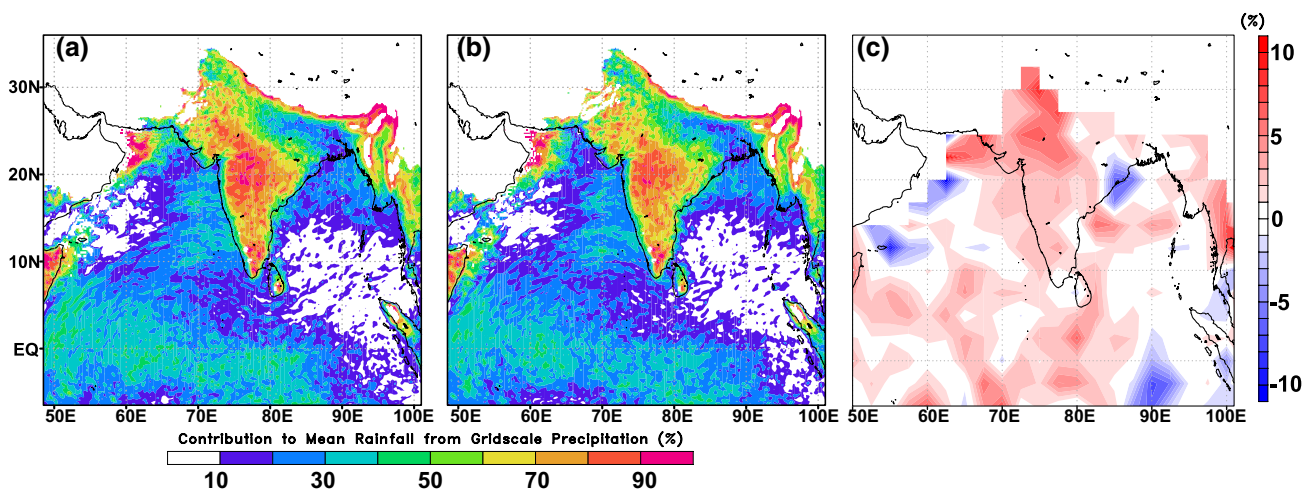


Fig. 9 The contribution to the total mean JJAS rainfall from grid-scale precipitation (%) in the **a** wIce and **b** woIce simulations. **c** The difference in grid-scale precipitation contribution between **a** and **b**

(wIce-woIce). The difference field was interpolated using area average with latitude weighting down to a $2.5^\circ \times 2.5^\circ$ grid

(explicit) precipitation and convective precipitation, we can analyze the impact on grid-scale precipitation through its contribution to the total precipitation. Note that grid-scale precipitation is generally dominant over land whereas over the Indian Ocean it contributes less (Fig. 9). Over central India, where grid-scale precipitation makes up at least 70% of the seasonal rainfall in many places, it was found that the contribution of the grid-scale precipitation increased further by 3–4% in wIce (Fig. 9c). Indeed, we observed an increase of 2–3% in grid-scale precipitation for the wIce simulations over most of the domain (Fig. 9c).

Exactly how much grid-scale rainfall was added relative to the convective rainfall and did this amount vary over India versus the Indian Ocean, recalling that grid-scale precipitation contributes less to the total over the ocean and ITCZ? One way to answer this would be to calculate the amount of rain that falls during JJAS in terms of volume to obtain a tangible understanding of how much seasonal rain the model produces. As shown in Fig. 10, the JJAS convective and grid-scale cumulative “rain volume” was calculated for India and equatorial Indian Ocean ITCZ (5°N–5°S and 65°E–95°E). Again, the convective rainfall plus the grid-scale rainfall make up the total model precipitation. In total precipitation, an increase in rain volume in the ITCZ was observed from woIce to wIce, whereas the rain volume was nearly unchanged over India. Notice that the grid-scale rain volume increased in both regions, as expected from Fig. 9,

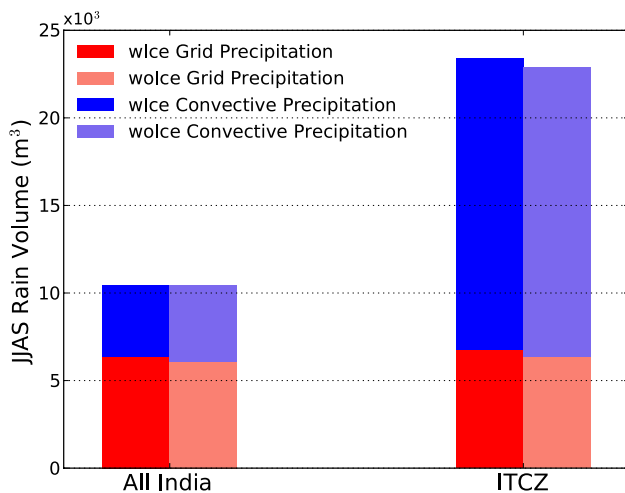


Fig. 10 The total amount of rainfall, delineated by the convective and grid-scale rain components, during the JJAS period measured in cubic meters of water ($\times 10^3$) over All India (land) and the ITCZ (defined here as 5°N–5°S and 65°E–95°E). Blue shading indicates the convective precipitation rain volume mean from the wIce simulations and the light blue shading indicates the same but from the woIce simulations. Red shading indicates the grid-scale precipitation rain volume mean from the wIce simulations and the light red indicates the same but from the woIce simulations. The total amount of rainfall equals the convective plus the grid-scale rainfall components

but that this does not translate to an increase in total rain volume over India and does so over the ITCZ. Over India the increase in grid-scale precipitation is compensated by a similar magnitude decrease in convective rainfall. Based on what is shown here, it is clear that at least a portion of the moisture removed from the model in the wIce runs is converted to grid-scale rainfall production through the cloud scheme and that it is observable from a mean seasonal perspective.

3.5 Multiyear simulations

It was desirable to conduct the wIce and woIce experiments a second time but letting the simulation progress for consecutive years instead of reinitializing every season because of the possibility that the results found in the seasonal runs are influenced by the selected simulation years and related spin-up issues. From Fig. 11 we see that the model mean seasonal rainfall cycle over All India is slightly increased in the wIce relative to woIce multiyear simulations. The peak difference in All India rainfall also coincides with the seasonal peak in rainfall in late July. Figure 12 shows the mean JJAS column integrated moisture or precipitable water, above the freezing level. Previously, in the seasonal runs we found a drying in the mid troposphere that was maximum near the freezing level in the wIce simulations. A similar result was found in the multi-year integrations where the precipitable water was consistently less by $\sim 0.5 \text{ kg/m}^2$ in wIce compared to woIce (Fig. 12). Because the region over India contains greater integrated moisture above the freezing level than the ITCZ, the change in precipitable water, between wIce and woIce, over India was greater than over the ITCZ (Fig. 12). The difference in moisture content above

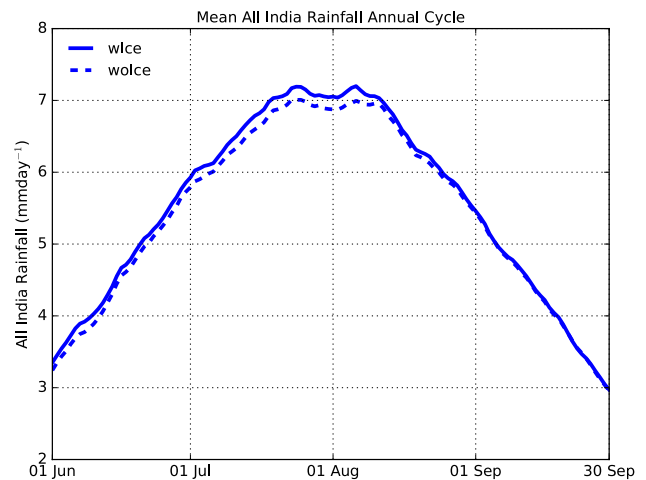


Fig. 11 The model mean daily rainfall averaged over All India during the summer monsoon in the wIce (solid blue line) and woIce (dashed blue line) multiyear simulations

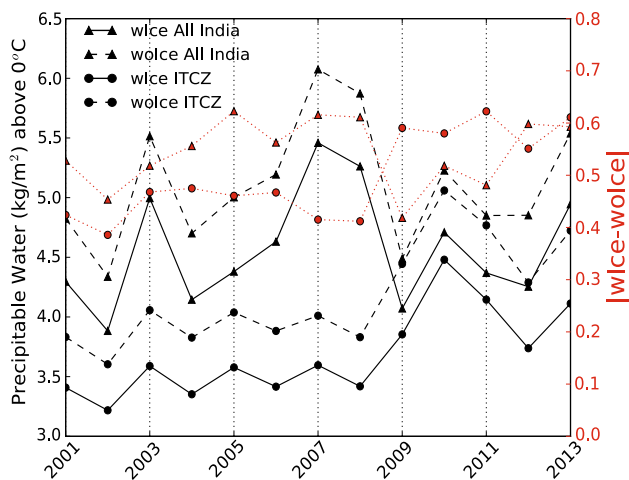


Fig. 12 The mean JJAS precipitable water found above the freezing level in the wIce and woIce multiyear simulations also over All India and the ITCZ (5°N–5°S and 65°E–95°E). The absolute difference in precipitable water between the wIce and woIce simulations is denoted by the dotted red lines for All India and the ITCZ. The solid black lines indicate the wIce multiyear simulation and the dashed black lines indicate the woIce multiyear simulation

the freezing level between wIce and woIce was generally constant throughout the multiyear simulations. Based on the results of the multiyear wIce and woIce experiments we find that the precipitation and moisture field differences as a result of SVP are largely unchanged when compared to the seasonal experiments.

To compliment the results from Sect. 3.4, Table 2 catalogs the mean and standard deviation statistics of the monsoon seasonal rainfall over All India and the ITCZ in the multiyear simulations compared with observations. The ITCZ rainfall was widely overestimated in both the wIce and woIce runs and the All India rainfall was underestimated, compared to GPCP and IMD observations. The standard deviation of the seasonal rainfall over All India was in better agreement with observations. Note that over India the wIce simulation adds to the mean seasonal rainfall variability slightly whereas over the ITCZ it dampens the variability. In agreement with Fig. 12, the mean seasonal rainfall difference between wIce and woIce indicated a slight increase in rainfall in wIce. Comparing the mean seasonal All India rainfall difference to the observed standard deviation in the

seasonal rainfall, we see that the mean difference between wIce and woIce (1.17 cm) is about 10% of the observed mean interannual variability of monsoon rainfall over India (8.08 cm in GPCP, 9.15 cm in IMD).

4 Summary and conclusions

This study examined the potential impact that the treatment of saturation vapor pressure (SVP) has on the Indian summer monsoon (ISM) using seasonal and multiyear simulations of the regional spectral model (RSM). Five monsoon seasons were simulated using the RSM; for each season, one simulation used liquid water saturation throughout (woIce) and one simulation used saturation over ice above the freezing level (wIce). Additionally, a multiyear simulation was conducted for each SVP setup, one wIce and one woIce. This study focused on the sensitivity that SVP has on the seasonal mean field of the ISM.

The seasonal cycle of the cloud layer amounts was examined in the seasonal simulations and compared with MODIS cloud observations. We found that the high-level cloud amount increased by 5–7% in all monsoon months in the wIce runs whereas the middle cloud amount decreased by 3–4% in wIce with respect to woIce. There was an underestimation of 10–15% in the low cloud fraction in both wIce and woIce across all seasons when comparing to MODIS observations.

When the saturation was set to over ice above the freezing level (wIce), a mean seasonal drying of specific humidity (q) occurred in the middle and upper troposphere. The maximum in drying in wIce was coincident with the location of the freezing level and the latitude of the maximum in q at the freezing level, which is over central India and the BoB. At the freezing level in the wIce runs, the saturation is changed to be over ice. This lowers the saturation specific humidity, bringing the air closer to saturation. The model responds by condensing more water out of the column and thereby decreasing q. In the model, when water vapor is condensed, owing to supersaturation, it falls out of the column in the form of precipitation. We expected then that grid-scale explicit precipitation would increase when SVP over ice was prescribed. We found that this was indeed the case and that this increase in grid-scale

Table 2 ITCZ and All india seasonal cumulative rainfall

| | IMD | GPCP | wIce | woIce | wIce-woIce |
|------|-------|---------------|---------------|----------------|----------------|
| Mean | 84.03 | 87.45 (76.95) | 68.11 (150.5) | 66.94 (148.74) | + 1.17 (+1.76) |
| SD | 9.15 | 8.08 (7.63) | 13.48 (31.53) | 13.10 (32.50) | 1.78 (1.96) |

Cumulative JJAS rainfall in cm. The wIce, woIce, and difference statistics were calculated from the multiyear simulation (2001–2013). IMD, India Meteorology Department rain gauge data from 1998 to 2003 (Rahman et al. 2009). GPCP, Global Precipitation Climate Project data from 1997 to 2011. Parenthesis indicate cumulative rainfall or standard deviation from the ITCZ (5°N–5°S and 65°E–95°E)

precipitation was present across most of the domain but was maximum over central India in the wIce runs. Over the equatorial Indian Ocean, the increase in grid-scale precipitation led to an increase in total mean rainfall. Over India however, the increase in grid-scale precipitation was compensated by a loss of convective precipitation and thus the total precipitation is nearly the same in wIce and woIce. The model responds to the slight decrease in the saturation condition above the freezing level in the wIce simulations by increasing grid-scale condensation of water above the freezing level and in doing so adds to a preexisting moisture sink in the model. Importantly, this added moisture sink, which acts to remove supersaturation, will be located in areas which contain relative humidities near 100%. Areas that are near 100% relative humidity (RH) with respect to water may be supersaturated with respect to ice, which will then result in removal of moisture. This implies that, during the ISM, areas over India that contain high mid-level relative humidities as a result of constant rainfall and convection will be most impacted by the removal of moisture that is triggered by SVP over ice above the freezing level. Indeed, we see in Fig. 6a, b that the region in which the most moisture is removed was over India. Mean seasonal mid-level RH in the ISM region was decreased in wIce relative to woIce, while upper-level RH increased in wIce relative to woIce. In mid-levels over most of the model domain this led to less seasonal cloudiness but more upper-level cloud amount relative to woIce. In terms of radiation then, seasonal solar radiation was increased in wIce at the surface due to less mid-level clouds. Terrestrial outgoing longwave radiation (OLR) increased at the top of the atmosphere (TOA) in wIce due to less absorption by the atmosphere and less mid-level cloudiness. The mean seasonal rainfall difference over India between wIce and woIce is around 10% of the observed interannual variability of seasonal All India rainfall.

A comparison between the seasonal and multiyear experiments showed that, qualitatively the impact of the imposed SVP difference on the mean precipitation and moisture fields is largely the same during the ISM. In the multiyear simulations we found that, consistent with the seasonal runs, the wIce precipitation over India was greater than in woIce. In terms of column moisture, the multiyear simulations corroborated the conclusions made from the seasonal runs by showing that the mean integrated moisture above the freezing level decreases in wIce. The SVP forcing appears to be a function of amount of moisture above the freezing level in the multiyear simulation.

In a future study, we plan to further explore the sensitivity of the monsoon climate to changes in SVP by including an interactive ocean component to the modeling system. This is warranted from the apparent changes to the surface

fluxes seen in this study that could have an impact on the upper ocean evolution and its interaction with the overlying atmosphere.

Acknowledgements The authors would like to thank the contributions of two anonymous reviewers to previous versions of the manuscript which greatly improved this study. The authors gratefully acknowledge the financial support given by the Earth System Science Organization, Ministry of Earth Sciences, Government of India (Grant number MM/SERP/FSU/2014/SSC-02/002) to conduct this research under Monsoon Mission. We thank the Indian Meteorological Department for the availability of the daily rain analysis over India. Computing resources were provided by the Texas Advanced Computing Center at the University of Texas and XSEDE under Grant number ATM10010 and Florida State University's High Performance Computer. The authors would also like to acknowledge Dr. Akhilesh Mishra at FSU COAPS for his advice and assistance in this work.

References

- Abhik S, Halder M, Mukhopadhyay P, Jiang X, Goswami BN (2013) A possible new mechanism for northward propagation of boreal summer intraseasonal oscillations based on TRMM and MERRA reanalysis. *Clim Dyn* 40:1611–1624
- Abhik S, Krishna RPM, Mahakur M, Ganai M, Mukhopadhyay P, Dudhia J (2017) Revised cloud processes to improve the mean and intraseasonal variability of the Indian summer monsoon in climate forecast system: part 1. *J Adv Model Earth Syst* 9:1002–1029
- Ashok K, Guan Z, Yamagata T (2001) Impact of the Indian Ocean dipole on the relationship between Indian monsoon rainfall and ENSO. *Geophys Res Lett* 28:4499–4502. <https://doi.org/10.1029/2001GLO13294>
- Bony S, Stevens B, Frierson DMW, Jakob C, Kageyama M, Pincus R, Shepherd TG, Sherwood SC, Siebesma AP, Sobel AH, Watanabe M, Webb MJ (2015) Clouds, circulation and climate sensitivity. *Nat Geosci* 8:261–268. <https://doi.org/10.1038/ngeo2398>
- Chang FL, Li Z (2005) A near-global climatology of single-layer and overlapped clouds and their optical properties retrieved from Terra/MODIS data using a new algorithm. *J Clim* 18:4752–4771
- Chou M-D (1992) A solar radiation model for use in climate studies. *J Atmos Sci* 49:762–772
- Chou M-D, Suarez MJ (1994) An efficient thermal infrared radiation parameterization for use in general circulation model. Technical report series on global modeling and data assimilation, NASA/TM-1994-104606, vol 3, p 85
- Dessler AE (2010) A determination of the cloud feedback from climate variations over the past decade. *Science* 330(6020):1523–1527. <https://doi.org/10.1126/science.1192546>
- Donner LJ, Wyman BL, Hemler RS, Horowitz LW, Ming Y, Zhao M, Golaz J, Ginoux P, Lin S, Schwarzkopf MD, Austin J, Alaka G, Cooke WF, Delworth TL, Freidenreich SM, Gordon CT, Griffies SM, Held IM, Hurlin WJ, Klein SA, Knutson TR, Langenhorst AR, Lee H, Lin Y, Magi BI, Malyshev SL, Milly PC, Naik V, Nath MJ, Pincus R, Ploshay JJ, Ramaswamy V, Seman CJ, Shevliakova E, Sirutis JJ, Stern WF, Stouffer RJ, Wilson RJ, Winton M, Wittenberg AT, Zeng F (2011) The dynamical core, physical parameterizations, and basic simulation characteristics of the atmospheric component AM3 of the GFDL global coupled model CM3. *J Clim* 24:3484–3519. <https://doi.org/10.1175/2011JCLI3955.1>
- Fowler LD, Randall DA, Rutledge SA (1996) Liquid and ice cloud microphysics in the CSU general circulation model. Part I: model description and simulated microphysical processes. *J Clim* 9:489–529

- Gettelman A, Collins WD, Fetzer EJ, Eldering A, Irion FW, Duffy PB, Bala G (2006) Climatology of upper-tropospheric relative humidity from the atmospheric infrared sounder and implication for climate. *J Clim* 19:6104–6120
- Giorgetta MA, Jungclaus J, Reick CH, Legutke S, Bader J, Böttinger M, Brovkin V, Cruieger T, Esch M, Fieg K, Glushak K, Gayler V, Haak H, Hollweg H-D, Ilyina T, Kinne S, Kornblueh L, Matei D, Mauritsen T, Mikolajewicz U, Mueller W, Notz D, Pithan F, Raddatz T, Rast S, Redler R, Roeckner E, Schmidt H, Schnur R, Segschneider J, Six KD, Stockhause M, Timmreck C, Wegner J, Widmann H, Wieners K-H, Claussen M, Marotzke J, Stevens B (2013) Climate and carbon cycle changes from 1850 to 2100 in MPI-ESM simulations for the coupled model inter-comparison project phase 5. *J Adv Model Earth Syst* 5:572–597. <https://doi.org/10.1002/jame.20038>
- Goswami BN (1998) Interannual variation of Indian summer monsoon in a GCM: external condition versus internal feedbacks. *J Clim* 11:501–522
- Goswami BB, Krishna RPM, Mukhopadhyay P, Khairoutdinov M, Goswami BN (2015) Simulation of the Indian summer monsoon in the superparameterized climate forecast system version 2: preliminary results. *J Clim* 28:8988–9012
- Hahn DG, J Shukla (1976) An apparent relationship between Eurasian snow cover and Indian monsoon rainfall. *J Atmos Sci* 33:2461–2462
- Huffman GJ, Bolvin DT, Adler RF (2012) GPCP version 1.2 1-degree daily (1DD) precipitation data set. World Data Center A, National climatic Data Center, Asheville
- Jiang X, Waliser DE, Li JL, Woods C (2011) Vertical cloud structures of the boreal summer intraseasonal variability based on CloudSat observations and ERA-interim reanalysis. *Clim Dyn* 36:2219–2232. <https://doi.org/10.1007/s00382-010-0853-8>
- Juang H-MH, Kanamitsu M (1994) The NMC nested regional spectral model. *Mon Weather Rev* 122.1:3–26
- Kanamaru H, Kanamitsu M (2007) Scale-selective bias correction in a downscaling of global reanalysis using a regional model. *Mon Weather Rev* 135:334–350
- Kanamitsu M, Ebisuzaki W, Woollen J, Yang S-K, Hnilo JJ, Fiorino M, Potter GL (2002) NCEP-DOE AMIP-II reanalysis. *Bull Am Meteorol Soc* 83:1631–1643
- Kanamitsu M, Yoshimura K, Yhang Y, Hong S (2010) Errors of interannual variability and multi-decadal trend in dynamical regional climate downscaling and its corrections. *J Geophys Res* 115:D17115
- Korolev A, Isaac GA (2006) Relative humidity in liquid, mixed-phase, and ice clouds. *J Atmos Sci* 63:2865–2880. <https://doi.org/10.1175/JAS3784.1>
- Korolev A, Mazin IP (2003) Supersaturation of water vapor in clouds. *J Atmos Sci* 60:2957–2974
- Krishnamurthy V, Shukla J (2000) Intraseasonal and interannual variability of rainfall over India. *J Clim* 13:4366–4377
- Krishnamurthy V, Shukla J (2007) Intraseasonal and seasonally persisting patterns of Indian monsoon rainfall. *J Clim* 20:3–20. <https://doi.org/10.1175/JCLI3981.1>
- Kumar S, Hazra A, Goswami BN (2014) Role of interaction between dynamics, thermodynamics and cloud microphysics on the summer monsoon precipitating cloud over the Myanmar Coast and the Western Ghats. *Clim Dyn* 43:911–924. <https://doi.org/10.1007/s00382-013-1909-3>
- Li H, Misra V (2014) Thirty-two-year ocean-atmosphere coupled downscaling of global reanalysis over the Intra-American Seas. *Clim Dyn* 43:2471–2489. <https://doi.org/10.1007/s00382-014-2069-9>
- Li H, Kanamitsu M, Hong S-Y, Yoshimura K, Cayan DR, Misra V (2013a) A high-resolution ocean-atmosphere coupled downscaling of a present climate over California. *Clim Dyn*. <https://doi.org/10.1007/s00382-013-1670-7>
- Li H, Kanamitsu M, Hong S-Y, Yoshimura K, Cayan DR, Misra V, Sun L (2013b) Projected climate change scenario over California by a regional ocean-atmosphere coupled model system. *Clim Change*. <https://doi.org/10.1007/s10584-013-1025-8>
- Liebmann B, Smith CA (1996) Description of a complete (interpolated) outgoing longwave radiation dataset. *Bull Am Meteorol Soc* 77:1275–1277
- Lohmann U, Roeckner E (1996) Design and performance of a new cloud microphysics scheme developed for the ECHAM general circulation model. *Clim Dyn* 12:557–572
- Marx L (2002) New calculation of saturation specific humidity and saturation vapor pressure in the COLA atmospheric general circulation model. COLA Tech Rep 130:1–23 (Available from the **Center for Ocean–Land–Atmosphere Studies, Calverton**)
- Matus AV, L'Ecuyer TS (2017) The role of cloud phase in Earth's radiation budget. *J Geophys Res Atmos* 122:2559–2578
- Meehl GA, Washington WM, Arblaster JM, Hu A, Teng H, Tebaldi C, Sanderson BN, Lamarque J, Conley A, Strand WG, White JB (2012) Climate system response to external forcings and climate change projections in CCSM4. *J Clim* 25:3661–3683. <https://doi.org/10.1175/JCLI-D-11-00240.1>
- Moorthi S, Suarez MJ (1992) Relaxed Arakawa–Schubert. A parameterization of moist convection for general circulation models. *Mon Weather Rev* 120:978–1002
- Moorthi S, Pan HL, Caplan P (2001) Changes to the 2001 NCEP operational MRF/AVN global analysis/forecast system. *NWS Tech Proced Bull* 484:14
- Murphy DM, Koop T (2005) Review of the vapor pressures of ice and supercooled water for atmospheric applications. *Q J R Meteorol Soc* 131:1539–1565. <https://doi.org/10.1256/qj.04.94>
- Murray BJ, O'Sullivan D, Atkinson JD, Webb ME (2012) Ice nucleation by particles immersed in supercooled cloud droplets. *Chem Soc Rev* 41:6519–6554
- Parthasarathy B, Munot AA, Kothawale DR (1994) All India monthly and seasonal rainfall series: 1871–1993. *Theor Appl Climatol* 49:217–224
- Platnick S, King MD, Ackerman SA, Menzel WP, Baum BA, Riedi JC, Frey RA (2003) The MODIS cloud products: Algorithms and examples from Terra. *IEEE Trans Geosci Remote Sens* 41:459–473
- Platnick S et al. (2015) MODIS atmosphere L3 daily product. NASA MODIS Adaptive Processing System, Goddard Space Flight Center, USA. https://doi.org/10.5067/MODIS/MOD08_D3.006
- Pruppacher HR, Klett JD (1978) Microphysics of clouds and precipitation. Reidel, Dordrecht
- Rahman SH, Sengupta D, Ravichandran M (2009) Variability of Indian summer monsoon rainfall in daily data from gauge and satellite. *J Geophys Res* 114:D17113
- Rajeevan M, Rohini P, Kumar KN, Srinivasan J, Unnikrishnan CK (2013) A study of vertical cloud structure of the Indian summer monsoon using CloudSat data. *Clim Dyn* 40:637–650. <https://doi.org/10.1007/s00382-012-1374-4>
- Ramanathan V (1987) The role of earth radiation budget studies in climate and general circulation research. *J Geophys Res* 92:4075–4095. <https://doi.org/10.1029/JD092iD04p04075>
- Ramanathan V, Cess RD, Harrison EF, Minnis P, Barkstrom BR, Ahmad E, Hartmann D (1989) Cloud-radiative forcing and climate: results from the earth radiation budget experiment. *Science* 243(4887): 57–63. <https://doi.org/10.1126/science.243.4887.57>
- Ramu DA, Sabeerali CT, Chattopadhyay R, Rao DN, George G, Dhakate AR, Salunke K, Srivastava A, Rao SA (2016) Indian summer monsoon rainfall simulation and prediction skill in the CFSv2 coupled model: impact of atmospheric horizontal resolution. *J Geophys Res* 121:2205–2221

- Randall DA et al (2007) Climate change 2007: the physical science basis. In: Solomon S et al (ed) Contributions of working group I to the fourth assessment report of the intergovernmental panel on climate change. Cambridge Univ. Press, Cambridge
- Rasmusson EM, Carpenter TH (1983) The relationship between the eastern Pacific seas surface temperature and rainfall over India and Sri Lanka. *Mon Weather Rev* 111:354–384
- Reynolds RW, Smith TM, Liu C, Chelton DB, Casey KS, Schlax MG (2007) Daily high-resolution blended analyses for sea surface temperature. *J Clim* 20:5473–5496
- Rossow WB, Schiffer RA (1991) ISCCP cloud data products. *Bull Am Meteor Soc* 72:2–20
- Rossow WB, Schiffer RA (1999) Advances in understanding clouds from ISCCP. *Bull Am Meteor Soc* 80:2261–2287
- Rotstajn LD, Ryan BF, Katzfey JJ (2000) A scheme for the calculation of the liquid fraction of mixed-phase stratiform clouds in large scale models. *Mon Weather Rev* 128:1070–1088. 10.1175/1520-0493(2000)128<1070:ASFCOT>2.0.CO;2
- Sabeerali CT, Rao SA, Dhakate AR, Salunke K, Goswami BN (2014) Why ensemble mean projection of south Asian monsoon rainfall by CMIP5 models is not reliable? *Clim Dyn* 45:161–174. <https://doi.org/10.1007/s00382-014-2269-3>
- Saha S, Moorthi S, Wu X, Wang J, Nadiga S, Tripp P, Behringer D, Hou Y, Chuang H, Iredell M, Ek M, Meng J, Yang R, Mendez MP, van den Dool H, Zhang Q, Wang W, Chen M, Becker E (2014) The NCEP climate forecast system version 2. *J Clim* 27:2185–2208. <https://doi.org/10.1175/JCLI-D-12-00823.1>
- Saji NH, Goswami BN, Vinayachandran PN, Yamagata T (1999) A dipole mode in the tropical Indian Ocean. *Nature* 401:360–363
- Schmidt GA, Kelley M, Nazarenko L, Ruedy R, Russell GL, Aleinov I, Bauer M, Bauer SE, Bhat MK, Bleck R, Canuto V, Chen Y-H, Cheng Y, Clune TL, Del Genio A, de Fainchtein R, Faluvegi G, Hansen JE, Healy RJ, Kiang NY, Koch D, Lacis AA, LeGrande AN, Lerner J, Lo KK, Matthews EE, Menon S, Miller RL, Oinas V, Oloso AO, Perlwitz JP, Puma MJ, Putman WM, Rind D, Romanou A, Sato M, Shindell DT, Sun S, Syed RA, Tausnev N, Tsigaridis K, Unger N, Voulgarakis A, Yao M-S, Zhang J (2014) Configuration and assessment of the GISS ModelE2 contributions to the CMIP5 archive. *J Adv Model Earth Syst* 6(1):141–184. <https://doi.org/10.1002/2013MS000265>
- Shimpo A, Kanamitsu M, Iacobellis S, Hong S-Y (2008) Comparison of four cloud schemes in simulating the seasonal mean field forced by the observed sea surface temperature. *Mon Weather Rev* 136:2557–2575
- Slingo JM (1980) A cloud parameterization scheme derived from GATE data for use with a numerical model. *Q J R Meteorol Soc* 106:747–770
- Slingo JM (1987) The development and verification of a cloud prediction scheme for the ECMWF model. *Q J R Meteorol Soc* 113:899–927
- Slingo A, Slingo JM (1991) Response of the National Center for Atmospheric Research Community Climate Model to improvements in the representation of clouds. *J Geophys Res* 96:341–357
- Sperber KR, Annamalai H, Kang IS, Kitoh A, Moise A, Turner A, Wang B, Zhou T (2012) The Asian summer monsoon: an inter-comparison of CMIP5 vs. CMIP3 simulations of the late 20th century. *Clim Dyn* 41:2711–2744. <https://doi.org/10.1007/s00382-012-1607-6>
- Stefanova L, Misra V, Chan S, Griffin M, O'Brien JJ, Smith III TJ (2012) A proxy for high-resolution regional analysis for the Southeast United States: assessment of precipitation variability in dynamically downscaled reanalyses. *Clim Dyn* 38:2449–2466. <https://doi.org/10.1007/s00382-011-1230-y>
- Stephens GL (2005) Cloud feedbacks in the climate system: a critical review. *J Clim* 18:237–273. <https://doi.org/10.1175/JCLI-3243.1>
- Su H, Jiang JH, Teixeira J, Gettelman A, Huang X, Stephens G, Vane D, Perun VS (2011) Comparison of regime-sorted tropical cloud profiles observed by CloudSat with GEOS5 analyses and two general circulation model simulations. *J Geophys Res* 116:D09104. <https://doi.org/10.1029/2010JD014971>
- Tan I, Storelvmo T, Zelinka MD (2016) Observational constraints on mixed-phase clouds imply higher climate sensitivity. *Science* 353:224–227
- Tremblay A, Glazer A (2000) An improved modeling scheme for freezing precipitation forecasts. *Mon Weather Rev* 128:1289–1308. 10.1175/1520-0493(2000)128<1289:AIMSFF>2.0.CO;2
- Waliser DE, Jin K, Kang IS, Stern WF, Schubert SD, Wu MLC, Lau KM, Lee MI, Krishnamurthy V, Kitoh A, Meehl GA, Galin VY, Satyan V, Mandke SK, Wu G, Liu Y, Park CK (2003) AGCM simulation of intraseasonal variability associated with the Asian summer monsoon. *Clim Dyn*. <https://doi.org/10.1007/s00382-003-0337-1>
- Waliser DE, Li JLF, Woods CP, Austin RT, Bacmeister J, Chern J, Del Genio A, Jiang JH, Kuang Z, Meng H, Minnis P, Platnick S, Rossow WB, Stephens GL, Sun-Mack S, Tao WK, Tompkins AM, Vane DG, Walker C, Wu D (2009) Cloud ice: a climate model challenge with signs and expectations of progress. *J Geophys Res* 114:D00A21. <https://doi.org/10.1029/2008JD010015>
- Waliser DE, Li J-LF, L'Ecuyer TS, Chen WT (2011) The impact of precipitating ice and snow on the radiation balance of global climate models. *Geophys Res Lett* 38:L06802. <https://doi.org/10.1029/2010GL046478>
- Wang T, Wong S, Fetzner EJ (2015) Cloud regime evolution in the Indian monsoon intraseasonal oscillation: connection to large-scale dynamical conditions and the atmospheric water budget. *Geophys Res Lett* 42:9465–9472. <https://doi.org/10.1002/2015GL066353>
- Weare BC (2004) A comparison of AMIP II model cloud layer properties with ISCCP D2 estimates. *Clim Dyn* 22:281–292
- Webster PJ, Magaña VO, Palmer TN, Shukla J, Tomas RA, Yanai M, Yasunari T (1998) Monsoons: processes, predictability, and the prospects for prediction. *J Geophys Res* 103:14451–14510
- WMO (1988) General meteorological standards and recommended practices, appendix A. Technical Regulations, WMO-No. 49. World Meteorological Organization, Geneva
- WMO (2015a) Measurement of upper-air pressure, temperature and humidity (J. Nash). Instruments and Observing Methods Report No. 121. Geneva
- WMO (2015b) Recommended algorithms for the computation of marine meteorological variables, I.6. JCOMM Technical Report No. 63. World Meteorological Organization, Geneva
- Wood R, Field PR (2000) Relationships between total water, condensed water, and cloud fraction in stratiform clouds examined using aircraft data. *J Atmos Sci* 57:1888–1905
- Xu K-M, Randall DA (1996) A semi-empirical cloudiness parameterization for use in climate models. *J Atmos Sci* 53:3084–3102
- Yau MK, Rogers RR (1989) A short course in cloud physics. In: Yau MK, Rogers RR (eds) Formation of cloud droplets, Ch. 6. Elsevier, Amsterdam